RESEARCH ARTICLE | NOVEMBER 01 2023

Aerothermal optimization of turbine cascade squealer tip with non-uniform squealer height

Hongzhi Cheng (程泓智) ; Hanzla Shahid (حنظلة شهيد) ; Shuyu Zhou (周书聿) ; Wei Wang (王伟) ; Quanyong Xu (徐全勇) ; Penghao Duan (段鹏浩)

Physics of Fluids 35, 116103 (2023)
https://doi.org/10.1063/5.0174610

Physics of Fluids ARTICLE pubs.aip.org/aip/pof

Aerothermal optimization of turbine cascade squealer tip with non-uniform squealer height

Cite as: Phys. Fluids **35**, 116103 (2023); doi: 10.1063/5.0174610
Submitted: 1 September 2023 · Accepted: 12 October 2023 ·
Published Online: 1 November 2023

Hongzhi Cheng (程泓智),[1,2,3] Hanzla Shahid (حنظلة شهيد),[1,4] Shuyu Zhou (周书聿),[5] Wei Wang (王伟),[6] Quanyong Xu (徐全勇),[5,a)] and Penghao Duan (段鹏浩)[1,a)]

AFFILIATIONS

[1]PHD Lab, Department of Mechanical Engineering, City University of Hong Kong, Hongkong 999077, China
[2]Laboratory of Light-Duty Gas-Turbine, Institute of Engineering Thermo-physics, Chinese Academy of Sciences, Beijing 100190, China
[3]School of Engineering Science, University of Chinese Academy of Sciences, Beijing 100049, China
[4]Department of Mechanical Engineering, School of Mechanical and Manufacturing Engineering, National University of Science and Technology, Islamabad 44000, Pakistan
[5]Institute for Aero Engine, Tsinghua University, Beijing 100084, China
[6]Department of Mechanical Engineering, The Hong Kong Polytechnic University, Hong Kong 999077, China

[a)]**Authors to whom correspondence should be addressed:** xuquanyong@tsinghua.edu.cn and pengduan@cityu.edu.hk

ABSTRACT

The squealer tip has significant influence on both the aerodynamic and heat transfer characteristics of the high-pressure turbine blade. However, due to the complexity of parameterization and meshing of the squealer and the complicated flow structure within the over-tip region, the existing squealer designs in the open literature have constant squealer heights. In this paper, the design space to the squealer height with non-uniform squealer height is extended and the new flow features it may bring are investigated. A parameterization system specifically designed for the non-uniform squealer height using five control parameters is implemented to automatically generate the geometry and hybrid meshes. Combining it with the multi-objective optimization system using genetic algorithms, a transonic turbine cascade squealer tip is optimized employing Reynolds-averaged Navier–Stokes k–ω shear stress transport model. The main objective of this study is to obtain a squealer configuration with the lowest total pressure loss coefficient and heat transfer coefficient. The optimum configuration with non-uniform squealer height achieves improvements in both the aerodynamic efficiency and the heat transfer performance, relative to the baseline conventional squealer tip geometry with the constant squealer height. Additionally, this work demonstrates that a flow structure in which the main flow forms a "blanket" below the leakage flow in the squealer is beneficial for aerothermal performance, especially reducing heat transfer losses, which provides valuable insight into the squealer tip design of advanced high-pressure turbines.

I. INTRODUCTION

Environmental and energy changes have brought enormous challenges to the world, and promoting green development has become a global consensus. Gas turbines are a critical power equipment that plays a vital role in modern energy production. Advanced gas turbine has a series of technical advantages[1–3] such as low fuel consumption rate, high reliability, low noise, and low emission, so it has become one of the research hotspots in the energy field.[4,5] The turbine tip leakage and the losses it causes have long been an essential factor affecting the turbine aerodynamic performance and have, therefore, received a great deal of attention. Many research works have shown that tip leakage losses in high-pressure turbines (HPTs) account for approximately one-third of the total losses in the blade channel.[6–8] Furthermore, the high temperature leakage flow can lead to high temperatures and heat loads on the walls of the tip area, which in turn threaten the reliability and lifetime of the turbine, as the airflow does not do any work on the turbine.[9,10] Therefore, how to effectively reduce blade tip leakage losses and thermal loads is one of the issues that must be taken into account in the design of high-efficiency and high-reliability HPTs.

To further reduce the leakage losses and heat load at the turbine blade tip, the squealer tip design scheme was proposed[8] and had been widely studied.[11–15] The blade squealer tip is a structure with single or multiple ribs added to the flat blade tip, using the combined effect of the ribs and the vortex structure within the squealers to achieve control

of leakage losses and heat transfer coefficients (HTCs). Ameri *et al.*[16] performed calculations to simulate the tip flow and heat transfer on a turbine blade with a squealer tip. The results indicated that the squealer tip strongly affected the heat transfer rate on the squealer surfaces, but had no significant effect on efficiency. Azad *et al.*[17] investigated the effect of a squealer tip geometry arrangement on HTC and static pressure distributions on a turbine cascade blade tip using a transient liquid crystal technique. Their results showed that the squealer geometry arrangement can change the leakage flow and HTCs, and a squealer on the suction side (SS) provided a better benefit compared to that on the pressure side (PS) or mid camber line. Key and arts[18] numerically and experimentally studied the tip leakage flow characteristics for flat and squealer turbine tip geometries at different Reynolds and Mach number conditions. They found that the squealer tip is relatively insensitive to changes in the Reynolds number, while an increase in the Reynolds number caused an increase in tip velocity levels for the flat tip. Schabowski and Hodson[19] investigated the impact of several combinations of squealer and winglet geometries on the turbine performance and also assessed the influence of the thickness of the squealers. They found that the squealers and their shape had a significant impact on the tip gap flow pattern and loss generation and a good agreement between computational fluid dynamics (CFD) and the experimental data.

These studies showed that, under the same operating conditions, the squealer tip had lower leakage losses and heat loads and was, therefore, an efficient and reliable design solution for the turbine tip geometry. Over the past few years, researchers have more deeply explored the mechanisms by which squealer tips control the aerothermal characteristics of leakage flow, and squealer tip technology has become widely used in gas turbines.[20–23] Zhang and He[24] provided an overview of recent progress in understanding HPT blade shroudless tip heat transfer and aerodynamics, especially in a transonic regime based on the experimental and numerical efforts. Their review highlighted some fundamental flow physics especially in high-speed over-tip leakage (OTL) flows. Lu *et al.*[25] evaluated two trailing edge cooling configurations and discussed their associated aerothermal characteristics. The results revealed that cooling the PS cutback tip was inefficient, while the SS cutback configuration was better cooled. Du *et al.*[26] numerically investigated the influence of the multi-cavity squealer tip on the blade tip and the over-tip casing aerothermal performance. The results indicated that the flat tip attained the largest thermal load on the blade tip and induced the largest total pressure loss, and the case with a single tip cavity achieved the smallest total pressure loss and HTC. Andreoli *et al.*[27] described a differential evolution strategy to perform a multi-objective optimization of the tip geometry of a cooled turbine blade. Their work demonstrated that the optimized tip geometries improved both the aerodynamic efficiency and heat load reduction relative to a conventional squealer tip arrangement. Duan and He[28] adopted a multi-objective genetic algorithm to optimize a turbine cascade squealer tip with varying squealer heights and tip cooling configurations. They found that the concurrent method obtained better aerodynamic efficiency and heat transfer performance than the conventional optimization, and the aerodynamic efficiency ranking was changed by adding cooling to the uncooled blades.

Despite some progress in understanding squealer tip regulation methods and mechanisms, most of the studies were mainly limited to investigate the influence of artificially set uniform squealer tips[16–18,23–25] on the aerothermal performance of HPTs. The effect of non-uniform turbine squealer tips using a multi-objective optimization approach needs to be explored in depth. In addition, the increasing temperature at the turbine inlet and leakage flow in recent years, as well as the unique flow characteristics of the transonic turbine tip that are different from subsonic flow, have increased the need to investigate the mechanism of non-uniform flutes and to carry out optimization. However, due to the complexity of the parameterization of the squealer itself and the short time for squealer tip research in transonic turbines, there has been little research into multi-objective optimization design of the transonic turbine squealer tip. To the best of the authors' knowledge, the only exception was the work by Andreoli *et al.*[27] who performed a multi-objective optimization of the tip geometry. In their work, the parameterization strategy generated arbitrary rim shapes around the coolant holes on the blade tip, and their results[27,29,30] revealed that the optimized uncooled tip geometries with special squealer designs showed significant benefits in terms of heat flux and efficiency. Nevertheless, their optimization strategy made it difficult to process such a turbine for verification in practice, and the optimization object is not a transonic turbine.

Given this, it is of great academic and engineering value to develop an effective framework for the parameterization and optimization of transonic HPT squealer tips and to explore the influence of non-uniform squealers on the aerothermal performance. The objective of this study is to obtain a squealer tip configuration with high aerothermal performance based on the simulation by a three-dimensional RANS solver. First, the experimental validation of the CFD calculation is presented, including aerodynamic and heat transfer characteristics. Then, the parameterization and optimization method are introduced to obtain some configurations with better aerothermal performance than the prototype turbine tip. Finally, a detailed flow field analysis is performed to gain a deeper understanding of how non-uniform squealer improves the tip performance, which is essential for the design and regulation of advanced HPTs.

The main contributions and novelties of this paper are summarized as follows:

- A methodology to parameterize fully arbitrary squealer shapes with a limited number of parameters is proposed.
- The automatic domain generation and meshing are robust to handle complex geometries while minimizing computation cost.
- A series of profiles are evaluated to identify an optimum configuration with best aerothermal performance.
- Compared with the baseline squealer geometry, the total pressure loss coefficient, leakage rate ratio, and HTC of the optimum configuration decrease by up to 4.55%, 25.08%, and 20.15%, respectively.
- A flow structure in which the main flow forms a "carpet" below the leakage flow in the squealer is found to be beneficial for significantly lowering the average HTC.

II. NUMERICAL METHODS AND OPTIMIZATION FRAMEWORK

A. Baseline geometry

This paper takes a scaled typical high-pressure turbine blade tested by Ma *et al.*[31] as the research object. The axial chord length (C_x)

TABLE I. Parameters of the cascade.

Design parameter	Value
Chord length C (mm)	54
Axial chord length C_x (mm)	39
Tip clearance h_t/s	1.0%
Cavity depth h_c/s	1.0%
Inlet turbulent intensity	1%
Inlet Reynolds number (based on C_x)	0.3×10^6
Exit Reynolds number (based on C_x)	0.9×10^6

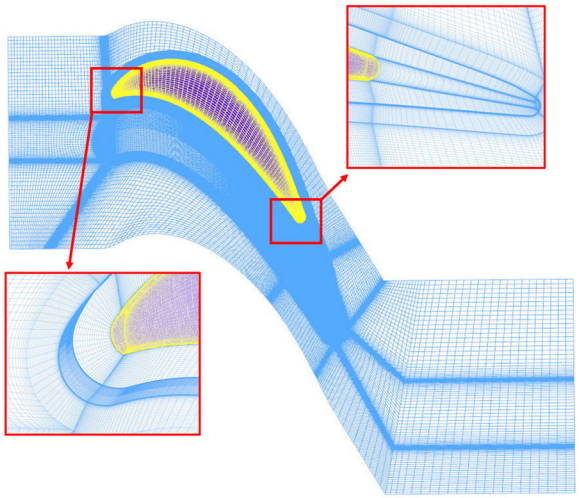

FIG. 1. Computational domain and mesh details.

of the cascade is 39 mm. Detailed geometric and aerodynamic parameters are listed in Table I.

B. Computational method and boundary conditions

In this study, the steady numerical simulations are conducted using the commercial solver ANSYS CFX. The code solves the 3D steady RANS equations based on the finite-volume method. The shear stress transport (k–ω *SST*) turbulence model is employed in this computation, because it considers the transport of the turbulent shear stress and predicts the complex flow phenomenon in the wall bounded flow.

The computational domain is a single-blade passage with periodic boundary condition, as shown in Fig. 1. The inlet total pressure ($P_{0,\text{in}}$) and total temperature ($T_{0,\text{in}}$) are set to 180 kPa and 300 K, respectively, and the outlet static pressure ($P_{s,\text{out}}$) is 101 kPa. The total pressure ($P_{0,c}$) and total temperature ($T_{0,c}$) at the coolant inlet are 198 kPa and 270 K, respectively. The injection angle is normal to the turbine squealer tip cavity floor. At the main flow inlet, the flow angle is 36.5°, and the turbulent intensity is 1%. The pressure difference between the inlet and outlet and the passage flow area variation make the outlet flow transonic. Overall, the boundary conditions and numerical setup are exactly the same with the previous studies.[31]

The HTC is computed by the Newton's law of cooling,

$$q = h(T_{ad} - T_w), \tag{1}$$

where q is the heat flux, T_w is the wall temperature, and T_{ad} is the adiabatic wall temperature. In the formula, q can be reconstructed by the impulse method developed by Oldfield.[32] h and T_{ad} are obtained from the linear regression between q and T_w. In the validation case, the HTC is computed by two cases with the isothermal wall temperature of 250 and 260 K.

C. Experimental validation of numerical simulation

Two types of squealer tip configurations are validated here: the uncooled blade and the blade with nine cooling holes on the tip cavity floor near the PS. The HTC contours on tip squealer were measured from the transient thermal data on a transonic wind tunnel, as depicted in Fig. 15(a). The test section including the coolant supply system is shown in Fig. 15(b). Figure 2 presents the HTC contours on the blade tip obtained from both experiments[31] and CFD including the uncooled and cooled cases. The calculated results are in qualitatively good agreement with the experimental data for all cases. Therefore, the geometric model and the numerical simulation methods employed in this research are successfully validated.

D. Mesh independence study

For the initial uncooled case with a uniform squealer height of 2%, four sets of structured hexahedral meshes are generated to study the mesh independence using the ICEM CFD. The O topology is utilized at the blade wall, tip clearance, and the squealer cavity. To ensure

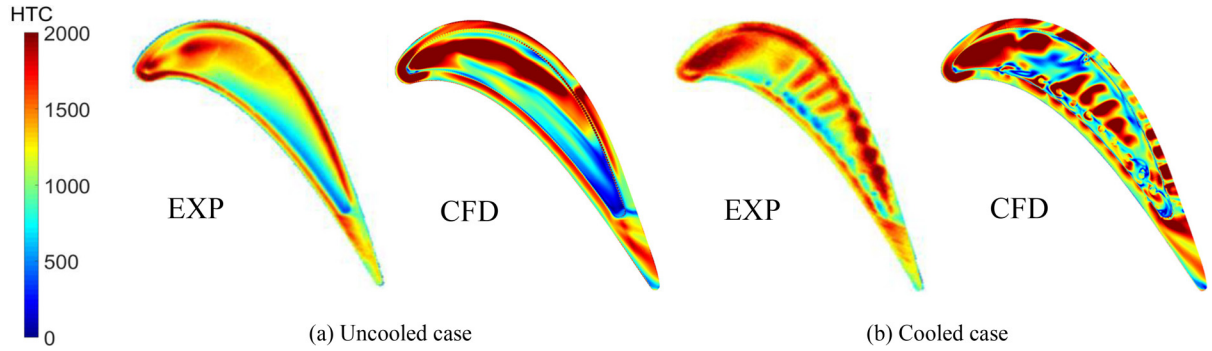

FIG. 2. Experimental validation[31] of HTC contours on the squealer tips.

TABLE II. Mesh study details.

	2×10^6	5×10^6	8×10^6	11×10^6
Nodes within tip clearance	15	20	25	30
Nodes within cavity depth	20	25	30	35
Average y^+	0.80	0.81	0.81	0.81
Average HTC W/(m^2 K)	1011	1052	1076	1079

TABLE III. Aerothermal performance parameters of different grids.

	σ	$\overline{HTC}$ ($Wm^{-2}K^{-1}$)
Pure hexahedral mesh	0.9627	1256.14
Hybrid mesh 1	0.9632	878.85
Hybrid mesh 2	0.9629	1463.47
Hybrid mesh 3	0.9631	1201.45
Pure tetrahedral mesh	0.9623	1133.05
HTC obtained by experiment		1199.1

that the average y^+ value on tip and cavity floor is less than 1, the grid height in the viscous sublayer region near the wall is set at 8×10^{-7} m. Furthermore, the overall grid quality is controlled above 0.3. Table II lists the calculated results of the four meshes. The simulated HTC value on the blade tip starts to change very little when the total mesh element number reaches 8×10^6. Therefore, the configuration of 8×10^6 structured hexahedral grids is considered acceptable for the simulation of the blade tip flow field.

However, the mesh quality of the squealer tip may drop when the squealer height varies significantly. Given this, the mixed mesh, with unstructured tetrahedral grid in the squealer region and structured hexahedral mesh in the rest of the computational domain, is utilized to improve the robustness and the quality of the mesh throughout the optimization process. In order to check the mesh independence, a total of three sizes of unstructured meshes are generated for the tip squealers, with the first layer of the boundary layer being 0.2 mm (marked as hybrid mesh 1), 0.1 mm (marked as hybrid mesh 2), and 0.06 mm (marked as hybrid mesh 3), respectively. In addition, a pure tetrahedral unstructured mesh with other parameters remaining the same as the pure hexahedral mesh is also generated for comparison. Figure 16 shows the cross sections of the squealer tip grids with different sizes. Table III displays the aerothermal performance parameters calculated by different grids under the adiabatic condition. The total pressure recovery coefficient (σ) and the total pressure loss coefficient (ζ) are defined in Eqs. (2) and (3), respectively.

Figure 3 shows the HTC contours of the squealer tips obtained from different grids. Since the results of the pure structured hexahedral mesh have been verified by the experimental data above, they are used as standard values for comparison with the calculation results of the other meshes. According to Table III, the unstructured grid has little influence on the aerodynamic performance, and the calculation results of the three hybrid grids and the pure tetrahedral grid are within the allowable range of error. However, it can be seen from Fig. 3 that the heat transfer performance is greatly affected. In Fig. 3, the HTC contour of the hybrid grid 3 [Fig. 3(d)] is the closest to the pure hexahedral grid [Fig. 3(a)], i.e., causes the least HTC error. Therefore, considering the aerodynamic and heat transfer performance comprehensively, the hybrid grid 3 is selected as the grid structure for follow-up research,

$$\sigma = P_{0,\mathrm{out}}/P_{0,\mathrm{in}}, \tag{2}$$

$$\zeta = (P_{0,\mathrm{in}} - P_{0,\mathrm{out}})/(P_{0,\mathrm{out}} - P_{s,\mathrm{out}}). \tag{3}$$

E. Parameterization of the squealer tip geometry

Figure 4 shows a schematic diagram of the parameterization of squealer. Three free parameters are used to control the squealer geometry: the squealer width, w_{sq}, the axial cutoff percentage, x_{sq}, and the squealer height, h_{sq}. The squealer curve is generated by drawing the normal lines perpendicular to the blade profiles with the length equaling to the squealer width of w_{sq}, and the squealer profile is cut off along the axial direction of the blade at the percentage of x_{sq}. Moreover, the squealer trailing edge at the location of x_{sq} is re-drawn using a circular curve. The squealer height is controlled by the squealer height, h_{sq}. These three parameters define squealer shapes to accommodate advanced turbine design requirements. In the previous research, the squealer height is uniform, i.e., constant h_{sq}, for any existing squealer design. However, in this study, the possibility of the squealer design with the non-uniform squealer height is investigated. The distribution of the

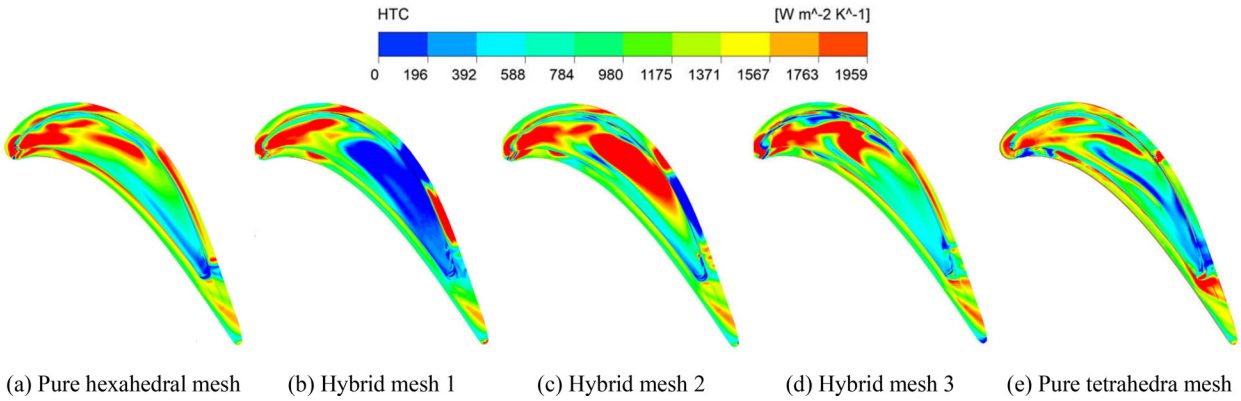

(a) Pure hexahedral mesh (b) Hybrid mesh 1 (c) Hybrid mesh 2 (d) Hybrid mesh 3 (e) Pure tetrahedra mesh

FIG. 3. The HTC contours of the squealer tips obtained from different grids.

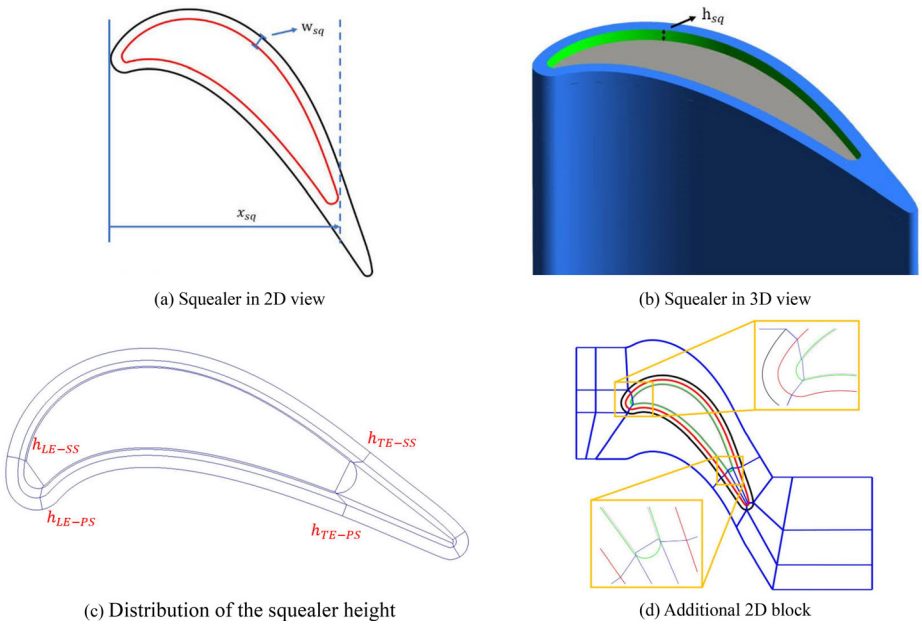

(a) Squealer in 2D view (b) Squealer in 3D view

(c) Distribution of the squealer height (d) Additional 2D block

FIG. 4. The schematic diagram of the parameterization of squealer.[33]

squealer height is controlled by four squealer heights at the leading edge-pressure side ($h_{\mathrm{LE-PS}}$), leading edge-suction side ($h_{\mathrm{LE-SS}}$), trailing edge-pressure side ($h_{\mathrm{TE-PS}}$), and trailing edge-suction side ($h_{\mathrm{TE-SS}}$). The distributions of the height between these four control points are interpolated linearly, as shown in Fig. 4(c). It is worth mentioning that the blocking system is modified to integrate the new design feature because of the additional o-block at the squealer, as shown in Fig. 4(d).

F. Multi-objective optimization strategy

In this study, the aerothermal performance of the turbine tip design is measured by two objectives: the total pressure loss coefficient ζ and the HTC. Therefore, a multi-objective strategy and algorithm is required to carry out this process. An improved non-dominated sorting genetic algorithm with an elite strategy (NSGA-II) is used to find a set of optimal solutions based on the concept of Pareto optimal frontier. The NSGA-II algorithm, proposed by Deb *et al.*,[34] is now one of the most widely used multi-objective genetic algorithms (MOGA).[35] Compared with the traditional MOGA, the NSGA-II has the characteristics of low algorithm complexity, high optimization efficiency, and avoiding partial optimization.[35] In addition, the NSGA-II provides a series of optimal solutions represented by the Pareto Front rather than one "best" solution, and it is extensively used in turbomachinery optimization.

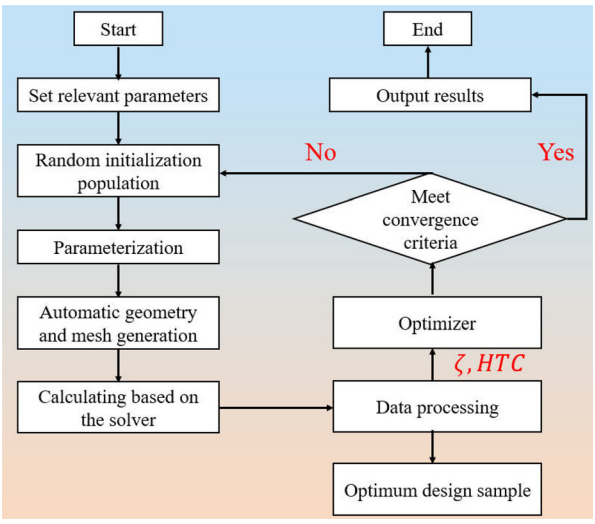

FIG. 5. Flowchart of the optimization process.

Figure 5 shows the flow chart of the optimization process. The steps are as follows: first, the design of experiments (DoEs) method is implemented to generate 30 individuals with varying squealer configurations. Second, the parameterization system is applied to obtain the geometry and the mesh of the 30 samples. Third, CFX is used to perform the numerical simulation and to output the two objectives of each design. Then, the data are normalized and input to the optimizer for the next iteration. Within the optimizer, the NSGA-II algorithm can figure out the ranking of the individuals based on the value of the two objectives and the spread of the solutions (crowding distance). According to the rank, the superior individuals are chosen to be the parents so that by cross-overing and mutating the parents' design feature represented by the chromosomes, the new individuals (offsprings) can be generated. In this study, each generation has ten new offsprings. By running the loop iteratively, the Pareto front is formed to obtain the optimal design, which combines both aerodynamic and heat transfer performance. The optimization is deemed to be converged when the optimal values of the two objectives do not change in two consecutive iterations. Finally, a series of optimal samples are obtained.

III. RESULTS AND DISCUSSION

A. Results and samples of the optimization process

In the sequential optimization process, as an initial DoEs, 30 turbine cascades with various non-uniform squealer height and axial

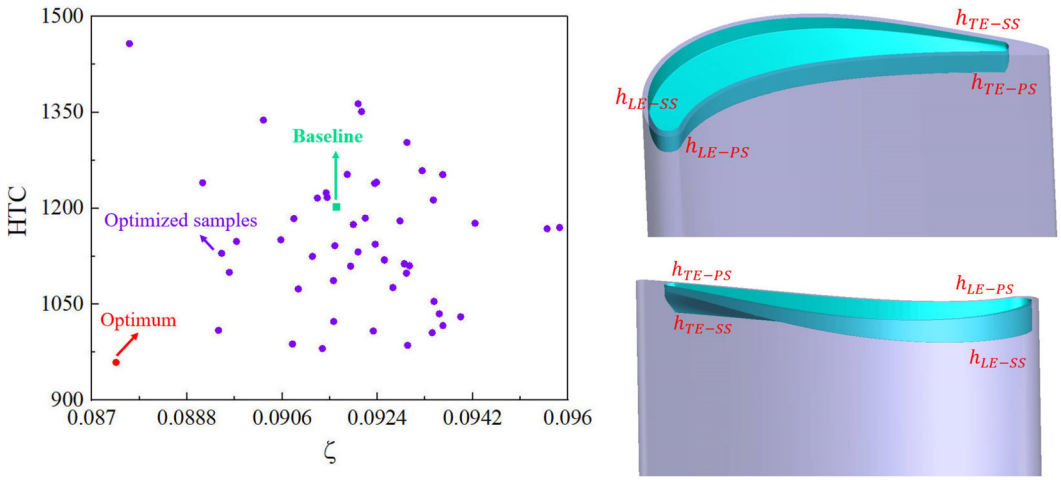

(a) Results of optimization (b) The tip squealer shape of the optimum sample

FIG. 6. The optimized samples and the optimum sample.

cutoff percentage are created. Subsequently, three iterations are run to explore the potential performance gain, and each iteration includes ten new squealer configurations. The optimization is stopped when the last two iterations do not bring additional performance improvement.

Figure 6(a) shows the results of the samples in terms of the optimization objectives, namely, the total pressure loss coefficient (ζ) and the HTC on the blade tip. The 60 individuals cover a varying range of 5% in aerodynamic loss and 20% in heat transfer. These optimized results suggest improved designs compared to the simple squealer performance, with ζ reductions up to 4.55% and tip HTC reductions up to 20.18%. It is worth mentioning that the optimal values of the two goals are reached at the same time, as indicated by the red circle in the figure. Figure 6(b) presents the non-uniform tip squealer shape of the optimum sample. The geometry introduces some features that may be common to all the tip squealer geometries with enhanced aerothermal performance.

This squealer with the optimum aerothermal performance has large squealer height at the leading edge-pressure side, leading edge-suction side, and trailing edge-pressure side, but much lower squealer height at the trailing edge-suction side, i.e., large $h_{\mathrm{LE-PS}}$, $h_{\mathrm{LE-SS}}$, $h_{\mathrm{TE-PS}}$ of 5.5%, and low $h_{\mathrm{TE-SS}}$ of 2%. Additionally, the squealer also has large axial cutoff percentage of 90%. From the perspective of aerodynamic performance, this configuration reduces the mass flow rate of the OTL flow, and thus the overall leakage loss. From the perspective of heat transfer, the LE squealer with an appropriate depth prevents the OTL flow from impinging to bottom of the squealer, and the reduction of OTL flow is also conducive to the smooth flow of the main stream in the squealer. Furthermore, at the TE, the slope of the squealer height between the PS and SS avoids strong heat exchange on the squealer floor. In general, the squealer tip configuration with this kind of design features significantly improves the aerothermal performance of the turbine cascade. More detailed analysis is given in Secs. III B–III E.

B. Aerodynamic performance and leakage characteristics

Modifications to the squealer geometry have a direct impact on the tip leakage characteristic due to the changing blockage effect, pressure distribution, and the flow structure of the OTL flow. Table IV compares the OTL mass flow rate and aerodynamic performance between the baseline and the optimum configuration. The tip OTL flow rates are normalized by the total inlet flow rate of the cascade.

As Table IV shows, the optimum design significantly decreases the OTL mass flow rate and the aerodynamic loss. This indicates that the mixing loss caused by the OTL flow can be significantly controlled by non-uniform squealer tip design. In the optimum case, the leakage rate ratio decreases substantially (25.08%), and thus, the total pressure loss coefficient decreases (4.55%).

C. Leakage characteristics and vortex dynamics

Figure 7 shows contours of normalized static entropy of the baseline geometry and optimum geometry in six spaced axial cutting planes. The cut planes are positioned at 20%, 30%, 40%, 60%, 80%, and 100% of the axial chord. This figure presents the influence of the OTL flow on the main flow and the corresponding mixing losses. At the fifth cut plane, there is a clearly visible region of high relative entropy near the tip caused by the OTL flow. This high relative entropy region coincides with the trace of the over-tip leakage vortex, which increases in size in the subsequent cut planes. The high-loss regions on the first four planes of the optimum configuration are larger than those on the original configuration, while the high-loss zones on the last two planes are significantly reduced. In addition, on the all cut planes, losses inside the squealer [marked in yellow in Fig. 7(b)] for the baseline geometry are significantly greater than the optimum

TABLE IV. Aerodynamic and tip leakage performance.

	Baseline configuration	Optimum configuration	Decreased degree (compared to baseline)
$m_{\mathrm{OTL}}/m_{\mathrm{in}}$	3.31%	2.48%	25.08%
ζ	0.092	0.087	5.43%

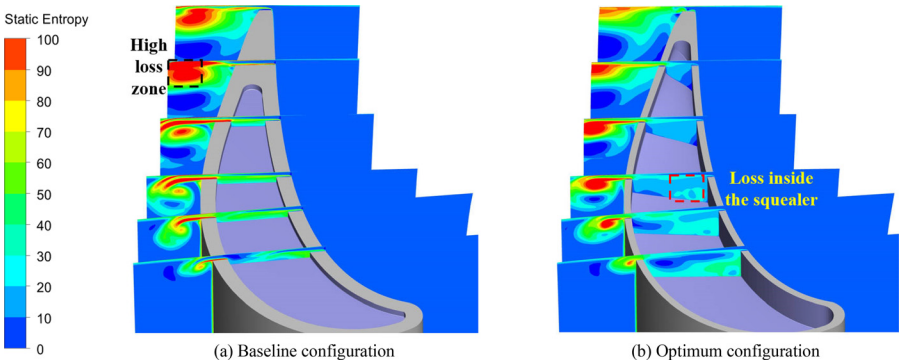

FIG. 7. Static entropy contours at different axial spans.

geometry, which has a significant impact on the tip aerodynamic performance.

To explore the characteristics of the OTL flow and the vortex structure in the tip region, Fig. 8 shows the streamlines of the OTL flow and the normalized axial vorticity contours on seven consecutive cutting planes starting at 10% of the axial chord. For these two configurations, there are two extremely large vorticity regions caused by tip leakage vortex (TLV) and induced vortex (IV). The induced vortex is formed due to the thickening of the wall shear layer caused by the TLV.[36] The two vortices constitute the vortex structure, and they jointly affect the turbine tip performance. As seen in Fig. 8(a), both the TLV and the IV are composed of two parts that flow through the squealer and outside of the squealer and develop from LE to TE of the blade. For the optimum geometry, the TLV inside the squealer near the LE is enhanced and reaches the blade SS in advance [the second cut plane in the Fig. 8(b)]. Similarly, the IV is formed earlier and reaches the blade SS faster. Therefore, the two vortex structures with opposite rational directions interacted earlier, leading to the increase in the high-loss regions in the first four sections in Fig. 7(b). However, the leakage fluid flows out of the squealer at the frontal portion of the blade, resulting in a significant decrease in the vortex intensity in the last five cut planes and early mixing of the TLV with the main flow. Because the Mach number at the frontal portion of the blade is lower, the mixing loss is substantially reduced. This early mixing of the TLV also leads to the smaller range of the TLV near the PS TE. Moreover, the upward slope of the squealer TE gradually "holds up" the main flow and changes the velocity direction of the main flow into the axial direction and the direction perpendicular to the axial direction, slowing down the collision with the end wall of the squealer when it flows out. This also helps to weaken the strength and scope of the TLV at the TE, as shown in the black box area in Fig. 8(b). These are mutually corroborated with the significantly decreased loss inside the squealer in the last five planes in Fig. 7(b).

Figure 9 shows the blade tip vortex structure captured by the Q-criterion and Fig. 10 gives the axial vortex contours in two LE planes, which jointly aids further identification and verification of the flow structures. Here, the Q value is adjusted to 3000 isosurface to show the vortex structure more clearly. It can be seen that the main vortex structures are basically consistent with the above-mentioned analysis based on Fig. 8, except that the suction side corner vortex near the blade LE. For the optimum geometry, in the squealer tip, the intensity of the TLV and IV near the LE are both increased, but they reach the blade SS faster, which significantly reduces the influence area of the vortex structure. Outside the squealer, the influence area of the vortex structure is also notably reduced due to the earlier arrival of the TLV and the decrease in the overall OTL flow. These all help promote a smooth flow of the mainstream, resulting in a significant reduction in overall aerodynamic losses.

Figure 11 shows the distribution of the pressure coefficient (C_p) at turbine tip span along the red line, which helps to further explore

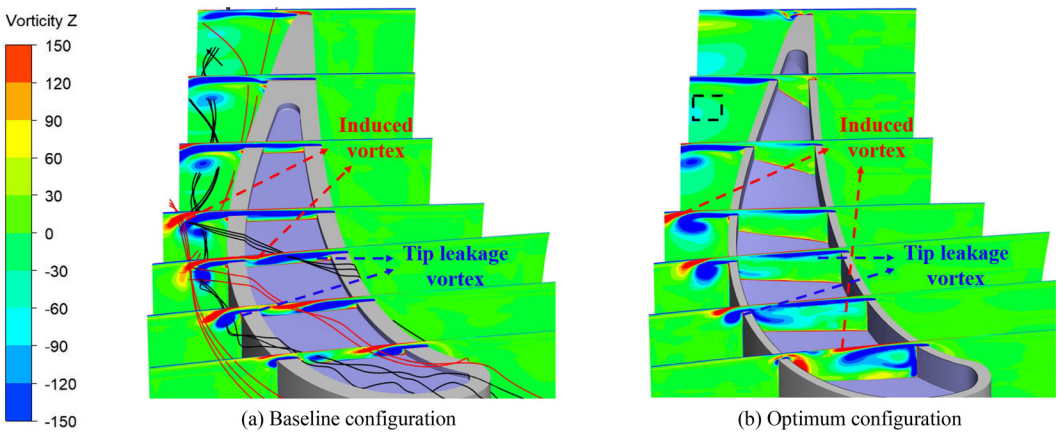

FIG. 8. Vortex structure and flow details of turbine tip.

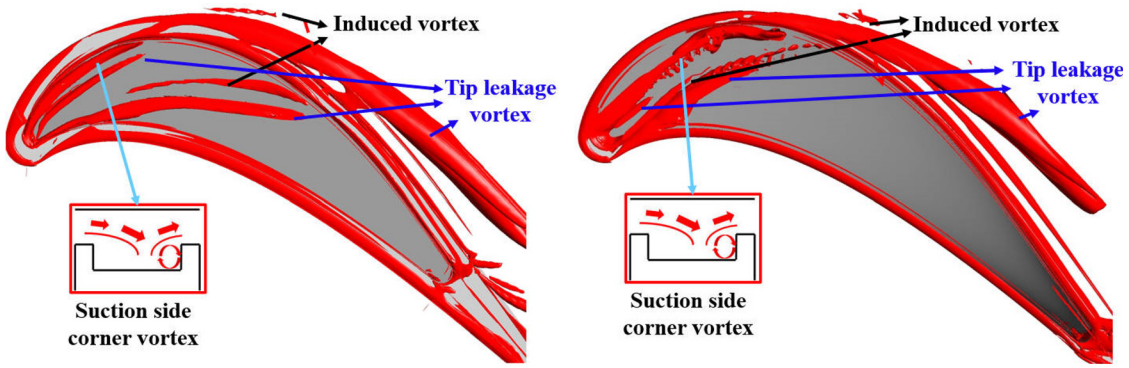

(a) Baseline configuration (b) Optimum configuration

FIG. 9. Identification of tip vortex structures based on Q-criterion.

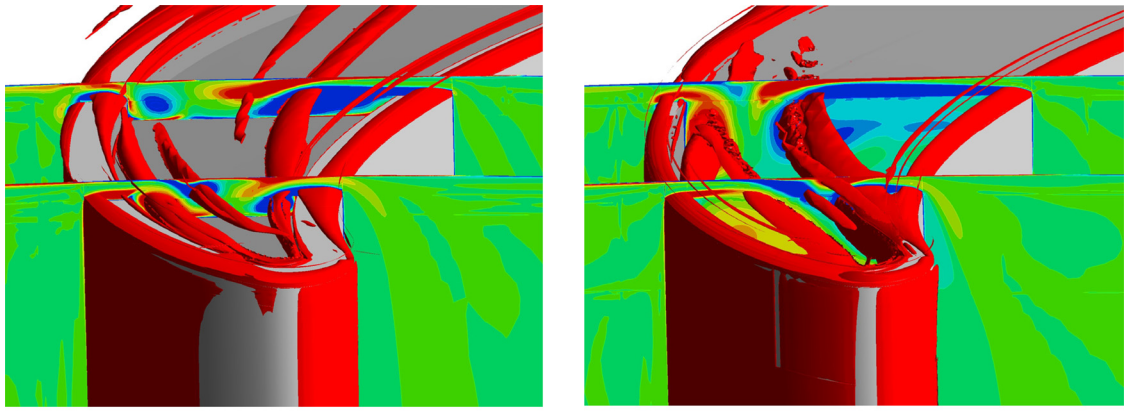

(a) Baseline configuration (b) Optimum configuration

FIG. 10. Vortex structures and contours of axial vortex.

and verify the cause of the change in the flow field. The pressure coefficient is defined as follows:

$$C_p = \frac{P_{\text{local}}}{\overline{P_{0,\text{in}}}}, \tag{4}$$

where P_{local} and $\overline{P_{0,\text{in}}}$ are the local static pressure and the average total pressure at the inlet, respectively.

As seen in Fig. 11(b), the pressure coefficient near the blade TE changes little, and the main changes exist at the blade LE and at the middle part of the blade. Specifically, for the baseline geometry, there is an obvious negative pressure zone (that is, C_p of the SS is greater than that of the PS) at the blade LE (0% C_x–20% C_x), which is not conducive to the outflow of the OTL but also intensifies the interaction between the OTL and the mainstream. For the optimum geometry, the negative pressure zone at the blade LE becomes a positive pressure zone, which promotes the LE OTL to flow out of the squealer quickly and reduces its interaction with the main flow. Moreover, the pressure difference between the PS and the SS remains basically constant in the middle of the blade (20% C_x–70% C_x), which is conducive to maintaining a stable flow state for the mainstream in the squealer after the OTL flows out.

D. Heat transfer characteristics

In Fig. 12, the distribution of the HTC on the squealer tip caps from different perspectives is depicted. For the baseline geometry, the HTC distribution shows a narrow band of high HTC consistent with the LE TLV trajectory. Similar to the OTL described previously, these high HTC bands move from the PS LE to the adjacent SS. After the arrival of the TLV, a high HTC zone is noticed at the squealer floor near the TE, as indicated by the black dashed. Based on the previous analysis, these high HTCs are caused by the interaction of the TLV and the IV and are maintained to the squealer floor TE.

In contrast to the baseline, the optimum geometry promotes a smooth flow of the mainstream within the squealer and achieves a significant reduction in average HTC. Specifically, although the intensity of the LE vortex system increases, the squealer with a certain depth avoids the strong interaction between the TLV and the bottom of the

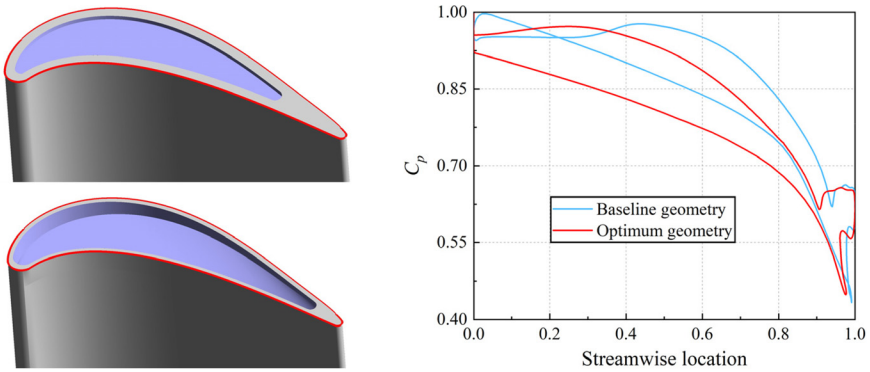

(a) The tip curve used to investigate the C_p (b) Pressure coefficient distributions of the tip

FIG. 11. Distributions of the pressure coefficient at the turbine tip curve.

squealer, thereby suppressing the increase in HTC. The area affected by the vortex structure is relatively concentrated, which is why the high HTC area in Fig. 12(b) is elliptical. Furthermore, near the TE region, the influence caused by the OTL is already very weak, and there is almost no interaction between the main flow and the squealer, so there is a significant low HTC zone (indicated by the red dashed). Similar to the bottom of the squealer, a significant HTC reduction is achieved in the TE region of the squealer floor. Therefore, this figure indicates that the HTC reductions are global rather than localized, and the variation of HTC is also consistent with the variation of tip flow field analyzed above.

E. Overall flow and entropy generation mechanism

Figure 13 presents the streamlines in the squealer of the optimum configuration to show the flow details more intuitively. As analyzed above, the flow near the squealer TE is smooth and is basically not disturbed by the vortex structure, and the main flow gradually rises until it finally flows out of the squealer. Near the squealer LE, although there is a strong vortex structure, the mainstream forms a layer of carpet at the bottom to support the vortex structure (as shown in the schematic diagram), avoiding the intense interaction between the bottom of the squealer and the vortex. In general, the optimum configuration well avoids the strong interaction between the fluid and the squealer and significantly reduces the aerodynamic loss and the average HTC.

This study can be considered to be carried out in a system where entropy is generated in turbulent flows with heat transfer, and the entropy transfer equation (Cartesian co-ordinates and Fourier heat conduction) is as follows:

$$\rho\left(\frac{\partial s}{\partial t}+u\frac{\partial s}{\partial x}+v\frac{\partial s}{\partial y}+w\frac{\partial s}{\partial z}\right)=\mathrm{div}\left(\frac{\vec{q}}{T}\right)+\frac{\Phi}{T}+\frac{\Phi_\Theta}{T^2}, \quad (5)$$

$$S_{\mathrm{gen}}=\frac{\Phi}{T}+\frac{\Phi_\Theta}{T^2}, \quad (6)$$

where s is the specific entropy, T is the thermodynamic temperature, and u, v, and w are the Cartesian velocity components. Φ/T and Φ_Θ/T^2 represent the entropy production by viscous dissipation and heat transfer, respectively, and S_{gen} represents the overall entropy generation.

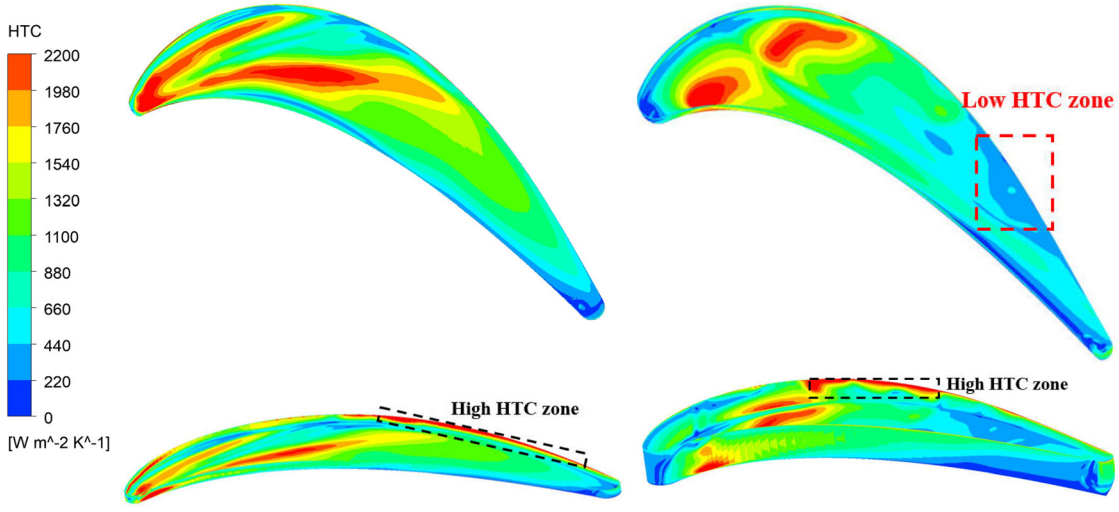

(a) Baseline configuration (b) Optimum configuration

FIG. 12. Contours of HTC on the blade squealer tip surfaces.

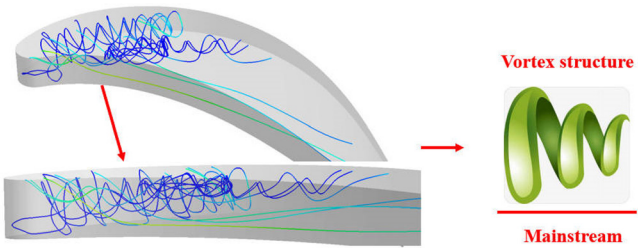

FIG. 13. Detailed streamlines in the squealer tip of the optimum geometry.

In general, the overall entropy generation is divided into two parts, that is, the entropy production due to viscous dissipation and that due to heat transfer dissipation. The specific expression and derivation process can be found in the literature.[37]

To analyze the flow loss more accurately and quantitatively, Fig. 14 shows the distribution of the viscosity and thermal dissipation within the squealer domain for the two geometries. It can be observed that the viscous dissipation and heat transfer dissipation of the optimum configuration are significantly lower than those of the baseline configuration. For the entropy production by viscous dissipation, the optimum geometry has a certain increase near the squealer LE (10% C_x–40% C_x) due to the enhancement of the TLV, but shows a significant decrease after the TLV flows out of the squealer (40% C_x–100% C_x), which is consistent with the conclusions obtained above. It is worth mentioning that the entropy production by heat transfer is quite unexpected but interesting, that is, the optimum configuration shows much lower average heat transfer dissipation than the baseline in the entire squealer. That is to say, the squealer structure that makes the main flow form a carpet under the TLV can effectively suppress the interaction between the TLV and the squealer, which has important reference meaning for the design of the turbine squealer tip.

IV. CONCLUSION

Squealer tip has been more and more widely used in HPTs due to its simple structure, good aerothermal performance, and suppression of OTL flow. Therefore, it is crucial to find an excellent squealer structure and clarify its effects and internal flow mechanism.

In this research, a method to parameterize fully arbitrary squealer shapes with a limited number of parameters is proposed, and on this basis, an optimization process is carried out to obtain an optimized transonic turbine cascade squealer tip. The optimizer uses NSGA-II to search the design space so that the two objectives, the total pressure loss coefficient and the HTC, are optimized by the variations of the squealer configurations. As the optimization converges, an optimum configuration with two best objectives is obtained, and a detailed flow field analysis is conducted to investigate the mechanism of the optimum squealer tip geometry. Some key results and conclusions can be drawn and summarized as follows:

(1) This optimization framework successfully obtains a squealer geometry with excellent aerothermal performance. Compared with the baseline configuration, the optimum configuration achieves a co-improvement in the aerothermal performance. The total pressure loss coefficient, leakage rate ratio, and HTC decrease by up to 4.55%, 25.08%, and 20.15%, respectively.
(2) Squealer geometry and tip loads have a significant effect on vortex structures. This configuration significantly reduces the influence range of the TLV and IV, thereby promoting the smooth flow of the mainstream near the squealer TE. In addition, the geometry suppresses the interaction between the TLV and the squealer floor. These together lead to a decrease in the OTL flow and a reduction in aerodynamic losses.
(3) The optimum configuration that makes the main flow form a carpet under the TLV can effectively suppress the shock and interaction of the OTL flow and TLV on the bottom of the squealer, which makes the average HTC in the squealer significantly reduced.
(4) The entropy generation analysis shows that the carpet structure greatly reduces the heat transfer dissipation in the squealer, and the overall descent degree is larger than that of the viscous dissipation, which is an unexpected but valuable finding.

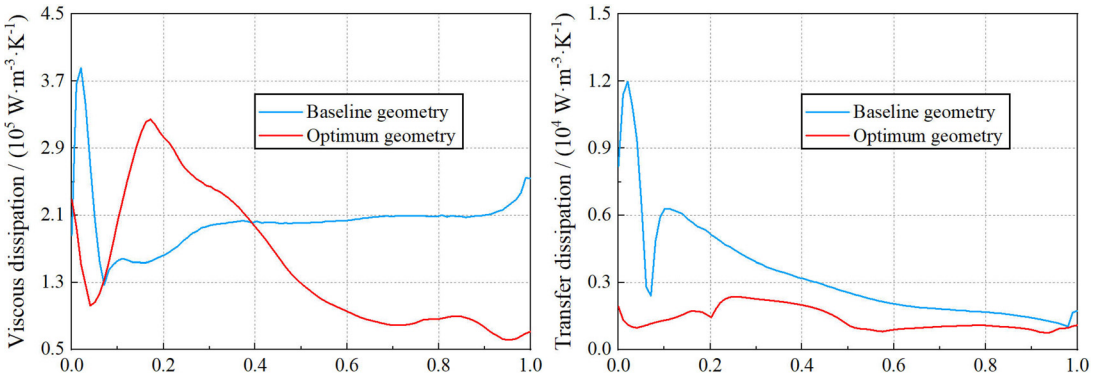

(a) Viscous dissipation (a) Thermal dissipation

FIG. 14. Viscous and thermal dissipation in the squealer.

Looking ahead, obtaining a HPT squealer tip with freely variable width and height is one of the engineering issues that must be addressed. In the future, this squealer configuration and optimization framework will be applied to turbine rotors and stages to further clarify its effects and will be tested experimentally to verify its actual aerothermal performance, which helps gain experience in the aerodynamic and thermal design of advanced HPTs.

ACKNOWLEDGMENTS

The authors acknowledge the financial support from the PI's start-up fund at the City University of Hong Kong (Grant No. 9610620), the Research Grants Council of the Hong Kong Special Administrative Region (Grant No. CityU 21206123), and the National Science and Technology Major Project of China (Grant Nos. J2019-V-0001-0092 and J2019-V-0013-0108).

AUTHOR DECLARATIONS

Conflict of Interest

The authors have no conflicts to disclose.

Author Contributions

Hongzhi Cheng: Investigation (equal); Methodology (equal); Writing – original draft (equal). **Hanzla Shahid:** Writing – review & editing (equal). **Shuyu Zhou:** Data curation (equal); Validation (equal). **Wei Wang:** Writing – review & editing (equal). **Quanyong Xu:** Software (equal); Supervision (equal). **Penghao Duan:** Conceptualization (equal); Formal analysis (equal); Supervision (equal); Writing – review & editing (equal).

DATA AVAILABILITY

The data that support the findings of this study are available within the article.

NOMENCLATURE

C_p	Pressure coefficient
C_x	Cascade chord length
CFD	Computational fluid dynamics
HPT	High-pressure turbine
HTC	Heat transfer coefficient
IV	Induced vortex
LE	Leading edge
MOGA	Multi-objective genetic algorithm
OTL	Over-tip leakage
$P_{0,in}$	Inlet total pressure
$P_{s,out}$	Outlet static pressure
PS	Pressure surface
Re	Reynolds number
RANS	Reynolds-averaged Navier–Stokes
SS	Suction surface
SST	Shear stress transport
$T_{0,in}$	Inlet total temperature
TE	Trailing edge
TLV	Tip leakage vortex
ζ	Total pressure loss coefficient
σ	Total pressure recovery coefficient

APPENDIX: NUMERICAL SIMULATION AND VALIDATION

Figures 15 and 16 presented the experimental facilities and the squealer tip hybrid mesh adopted in this study.

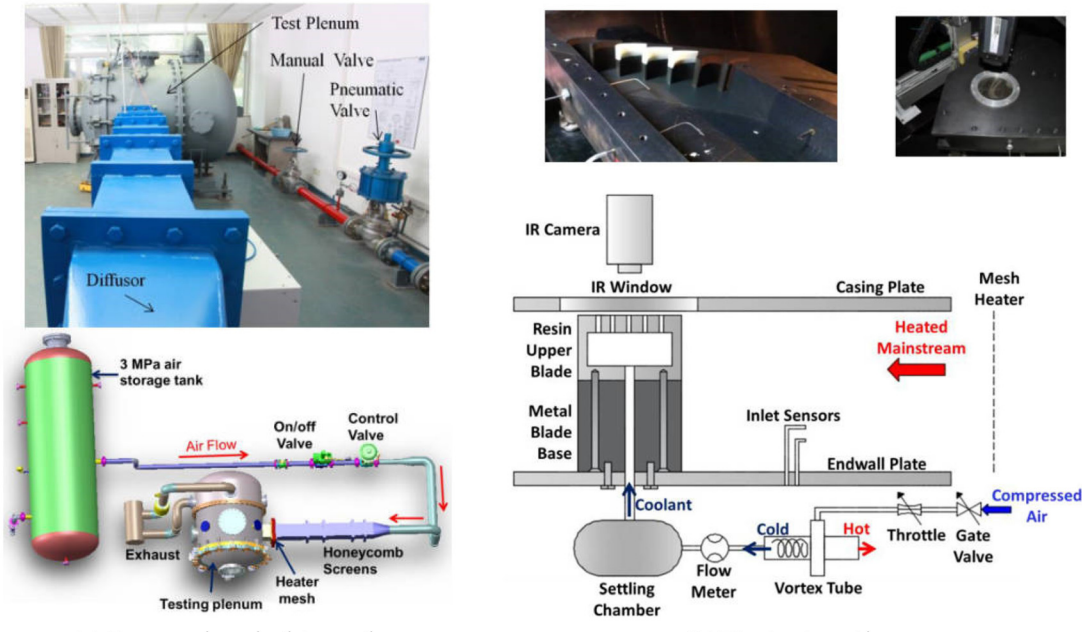

(a) Transonic wind tunnel. (b) The test section

FIG. 15. Experimental facilities adopted in this study.[24]

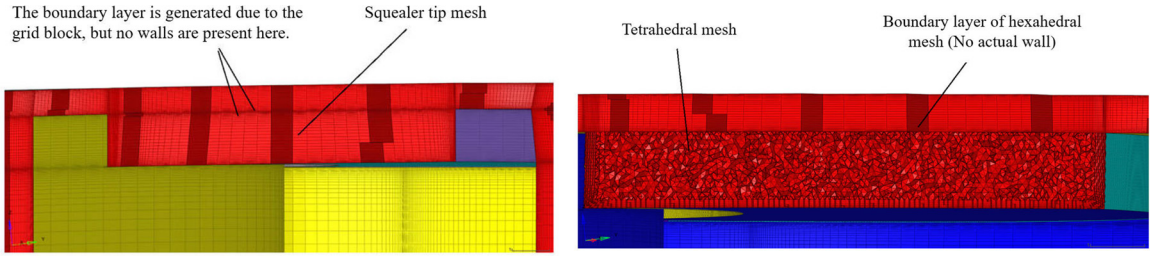

(a) Pure hexahedral mesh (b) Hybrid mesh with a basic notch size of 0.06 mm

FIG. 16. The schematic cross sections of the squealer tip grids with different sizes.

REFERENCES

[1]Y. X. Liu, B. Y. Lu, X. Z. Kong *et al.*, "Effects of the misalignment and axial gap on performance of a cover-plate pre-swirl system with impellers for gas turbine cooling," Phys. Fluids **35**, 105110 (2023).

[2]Z. L. Li, G. Han, C. X. Zhou *et al.*, "Quantitative analysis on influence of secondary flow for centrifugal impeller internal flow," Phys. Fluids **35**, 076113 (2023).

[3]H. Z. Cheng, Z. L. Li, P. H. Duan *et al.*, "Robust optimization and uncertainty quantification of a micro axial compressor for unmanned aerial vehicles," Appl. Energy **352**, 121972 (2023).

[4]H. Z. Cheng, C. X. Zhou, Z. L. Li *et al.*, "Robust aerodynamic optimization and design exploration of a wide-chord transonic fan under geometric and operational uncertainties," Energy **278**, 128011 (2023).

[5]H. Z. Cheng, C. X. Zhou, Z. L. Li *et al.*, "Uncertainty quantification and sensitivity analysis on the aerodynamic performance of a micro transonic compressor," Aerosp. Sci. Technol. **141**, 108569 (2023).

[6]J. D. Denton, "Loss mechanisms in turbomachines," J. Turbomach. **115**(4), 621–656 (1993).

[7]J. Moore and J. S. Tilton, "Tip leakage flow in a linear turbine cascade," J. Turbomach. **110**(1), 18–26 (1988).

[8]R. S. Bunker, "Axial turbine blade tips: Function, design, and durability," J. Propul. Power **22**(2), 271–285 (2006).

[9]R. S. Bunker, "A review of turbine blade tip heat transfer," Ann. N. Y. Acad. Sci. **934**(1), 64–79 (2001).

[10]P. H. Duan and L. He, "Application of multiscale methodology for transonic turbine blade tip cooling design," J. Turbomach. **142**(8), 081011 (2020).

[11]C. D. Maesschalck, V. Anderoli, G. Paniagua *et al.*, "Aerothermal optimization of turbine squealer tip geometries with arbitrary cooling injection," J. Turbomach. **143**(11), 111010 (2021).

[12]J. Vieria, J. Coull, P. Ireland *et al.*, "Aerothermal effect of cavity welding beads on a transonic squealer tip," J. Turbomach. **143**(11), 111009 (2021).

[13]W. Q. Tang, G. T. Shi, Y. X. Xiao *et al.*, "Study on the blade squealer tip affecting tip leakage flow and performance of a multiphase pump," Phys. Fluids **35**(2), 025137 (2023).

[14]Z. Y. Shao, H. Y. Zhang, and R. N. Wang, "Development and loss mechanism of turbine secondary flows at a low Reynolds number: A synergy analysis," Phys. Fluids **35**(10), 105101 (2023).

[15]L. Huang, Z. P. Zou, C. Fu *et al.*, "Impact of complex flow structures on the turbine blade tip region mixing," Phys. Fluids **35**(1), 015119 (2023).

[16]A. A. Ameri, E. Steinthorsson, and D. L. Rigby, "Effect of squealer tip on rotor heat transfer and efficiency," J. Turbomach. **120**(4), 753–759 (1998).

[17]G. S. Azad, J. C. Han, R. S. Bunker *et al.*, "Effect of squealer geometry arrangement on a gas turbine blade tip heat transfer," J. Heat Transfer **124**(3), 452–459 (2002).

[18]N. L. Key and T. Arts, "Comparison of turbine tip leakage flow for flat tip and squealer tip geometries at high-speed conditions," J. Turbomach. **128**(2), 213–220 (2006).

[19]Z. Schabowski and H. Hodson, "The reduction of over tip leakage loss in unshrouded axial turbines using winglets and squealers," J. Turbomach. **136**(4), 041001 (2014).

[20]Y. B. Wang, Y. P. Song, J. Y. Yu *et al.*, "Effect of cooling injection on the leakage flow of a turbine cascade with honeycomb tip," Appl. Therm. Eng. **133**, 690–703 (2018).

[21]X. J. He, Z. P. Zou, L. C. Yao *et al.*, "Refined flow organization in squealer tip gap and its impact on turbine aerodynamic performance," Aerosp. Sci. Technol. **138**(7), 108331 (2023).

[22]Y. J. Chen, L. Cai, D. Y. Jiang *et al.*, "Experimental and numerical investigations for turbine aerodynamic performance with different pressure side squealers and incidence angles," Aerosp. Sci. Technol. **136**(5), 108234 (2023).

[23]Y. F. Wang, W. H. Zhang, D. M. Huang *et al.*, "Control strategies for tip leakage vortex using inclined squealer rim in axial turbines," Phys. Fluids **34**(3), 036101 (2022).

[24]Q. Zhang and L. He, "Turbine blade tip aero-thermal management: Some recent advances and research outlook," J. Global Power Propul. Soc. **1**(4), 271–287 (2017).

[25]S. Lu, H. Ma, Q. Zhang *et al.*, "Cutback squealer tip trailing edge cooling performance," Int. J. Heat Fluid Flow **154**, 119632 (2020).

[26]K. Du, Z. G. Li, J. Li *et al.*, "Influences of a multi-cavity tip on the blade tip and the over tip casing aerothermal performance in a high pressure turbine cascade," Appl. Therm. Eng. **147**, 347–360 (2019).

[27]V. Andreoli, J. Braun, G. Paniagua *et al.*, "Aerothermal optimization of fully cooled turbine blade tips," J. Turbomach. **141**(6), 061007 (2019).

[28]P. H. Duan and L. He, "Optimization of turbine cascade squealer tip cooling design by combining shaping and flow injection," J. Turbomach. **143**(11), 111007 (2021).

[29]B. C. Cernat, M. Pátý, C. D. Maesschalck *et al.*, "Experimental and numerical investigation of optimized blade tip shapes—Part I: Turbine rainbow rotor testing and numerical methods," J. Turbomach. **141**(1), 011006 (2019).

[30]M. Pátý, B. C. Cernat, C. D. Maesschalck *et al.*, "Experimental and numerical investigation of optimized blade tip shapes—Part II: Tip flow analysis and loss mechanisms," J. Turbomach. **141**(1), 011007 (2019).

[31]H. Ma, Q. Zhang, L. He *et al.*, "Cooling injection effect on a transonic squealer tip—Part I: Experimental heat transfer results and CFD validation," J. Eng. Gas Turbines Power **139**(5), 052506 (2017).

[32]M. L. G. Oldfield, "Impulse response processing of transient heat transfer gauge signals," J. Turbomach. **130**(2), 021023 (2008).

[33]P. H. Duan, "Turbine design combining shaping and flow injection by using multiscale methodology," Ph.D. dissertation (Oxford University, Oxford, 2021).

[34]K. Deb, A. Pratap, S. Agarwal *et al.*, "A fast and elitist multiobjective genetic algorithm: NSGA-II," IEEE Trans. Evol. Comput. **6**(2), 182–197 (2002).

[35]C. Poloni, A. Giurgevich, L. Onesti *et al.*, "Hybridization of a multi-objective genetic algorithm, a neural network and a classical optimizer for a complex design problem in fluid dynamics," Comput. Methods Appl. Mech. Eng. **186**(2–4), 403–420 (2000).

[36]D. E. Van Zante, A. J. Strazisar, J. R. Wood *et al.*, "Recommendations for achieving numerical simulation of tip clearance flows in transonic compressor rotors," J. Turbomach. **122**(10), 733 (2000).

[37]H. Z. Cheng, Z. L. Li, C. X. Zhou *et al.*, "Effect of blade surface cooling on a micro transonic axial compressor performance at low Reynolds number," Appl. Therm. Eng. **226**(5), 120353 (2023).